HHS Public Access

Author manuscript

J Am Chem Soc. Author manuscript; available in PMC 2024 October 01.

Published in final edited form as:

J Am Chem Soc. 2023 July 05; 145(26): 14276–14287. doi:10.1021/jacs.3c02520.

Development and Validation of Nerve-Targeted Bacteriochlorin Sensors

Javier Hernández-Gil[††],
Department of Radiology, Memorial Sloan Kettering Cancer Center, New York, New York 10065, United States

Biomedical MRI/MoSAIC, Department of Imaging and Pathology, Katholieke Universiteit Leuven, B3000 Leuven, Belgium

Instituto de Tecnología Química, Universitat Politècnica de València, Consejo Superior de Investigaciones Científicas, Valencia E-46022, Spain

Chun Yuen Chow[††],
Institute for Molecular Bioscience and Australian Research Council Centre of Excellence for Innovations in Peptide and Protein Research, The University of Queensland, St Lucia, Queensland 4072, Australia

Hugo Chatras,
Department of Chemistry, Cleveland State University, Cleveland, Ohio 44115, United States

Paula Demétrio de Souza França,
Department of Radiology, Memorial Sloan Kettering Cancer Center, New York, New York 10065, United States

Department of Otorhinolaryngology and Head and Neck Surgery, Federal University of São Paulo, São Paulo, SP 04020-041, Brazil

[*]**Corresponding Authors: Thomas Reiner** – *Department of Radiology, Memorial Sloan Kettering Cancer Center, New York, New York 10065, United States; Department of Pharmacology, Weill-Cornell Medical College, New York, New York 10065, United States; Molecular Pharmacology Program, Memorial Sloan Kettering Cancer Center, New York, New York 10065, United States; Department of Radiology, Weill Cornell Medical College, New York, New York 10065, United States;* reinert@mskcc.org; Fax: 646 422 0408, **Junior Gonzales** – *Department of Radiology, Memorial Sloan Kettering Cancer Center, New York, New York 10065, United States; Department of Chemistry, Cleveland State University, Cleveland, Ohio 44115, United States; Center for Gene Regulation in Health and Disease, Cleveland, Ohio 44115, United States;* j.gonzales22@csuohio.edu; Fax: 216 687 2473.

[††]Author Contributions

J.H.G. and C.Y.C. contributed equally.

Notes

The authors declare the following competing financial interest(s): T.R. and J.S.L. are shareholders of Summit Biomedical Imaging, LLC. T.R. is a paid consultant for Theragnostics, Inc. T.R. is now an employee and a shareholder of Evergreen Theragnostics. All other authors have no conflict to declare. This arrangement has been reviewed and approved by CSU and MSK in accordance with its conflict-of-interest policies. P.D.S.F., J.G, J.L., T.R., and G.F.K. are co-inventors on a US patent. The Hs1a peptide has been optioned to Quaero Pharma.

Complete contact information is available at: https://pubs.acs.org/10.1021/jacs.3c02520

ASSOCIATED CONTENT

Supporting Information

The Supporting Information is available free of charge at https://pubs.acs.org/doi/10.1021/jacs.3c02520.

Detailed experiments and methods, synthetic protocols, chemical conjugations, standard characterization, figures, NMR spectra, HPLC purity analysis, LCMS analysis, tryptic digests, cell culture, whole-cell patch-clamp electrophysiology, mouse animal models, H&E and IHC histology, fresh confocal microscopy and corresponding epifluorescence, Cerenkov and PET imaging (PDF)

Zachary V. Samuels,
Department of Radiology, Memorial Sloan Kettering Cancer Center, New York, New York 10065, United States

Mike Cornejo,
Department of Radiology, Memorial Sloan Kettering Cancer Center, New York, New York 10065, United States

Glenn F. King,
Institute for Molecular Bioscience and Australian Research Council Centre of Excellence for Innovations in Peptide and Protein Research, The University of Queensland, St Lucia, Queensland 4072, Australia

Jason S. Lewis,
Department of Radiology, Memorial Sloan Kettering Cancer Center, New York, New York 10065, United States

Department of Pharmacology, Weill-Cornell Medical College, New York, New York 10065, United States

Molecular Pharmacology Program, Memorial Sloan Kettering Cancer Center, New York, New York 10065, United States

Department of Radiology, Weill Cornell Medical College, New York, New York 10065, United States

Thomas Reiner*,
Department of Radiology, Memorial Sloan Kettering Cancer Center, New York, New York 10065, United States

Department of Pharmacology, Weill-Cornell Medical College, New York, New York 10065, United States

Molecular Pharmacology Program, Memorial Sloan Kettering Cancer Center, New York, New York 10065, United States

Department of Radiology, Weill Cornell Medical College, New York, New York 10065, United States

Junior Gonzales*
Department of Radiology, Memorial Sloan Kettering Cancer Center, New York, New York 10065, United States

Department of Chemistry, Cleveland State University, Cleveland, Ohio 44115, United States

Center for Gene Regulation in Health and Disease, Cleveland, Ohio 44115, United States

Abstract

We report an innovative approach to producing bacteriochlorins (bacs) via formal cycloaddition by subjecting a porphyrin to a trimolecular reaction. Bacs are near-infrared probes with the intrinsic ability to serve in multimodal imaging. However, despite their ability to fluoresce and chelate metal ions, existing bacs have thus offered limited ability to label biomolecules for

target specificity or have lacked chemical purity, limiting their use in bio-imaging. In this work, bacs allowed a precise and controlled appending of clickable linkers, lending the porphyrinoids substantially more chemical stability, clickability, and solubility, rendering them more suitable for preclinical investigation. Our bac probes enable the targeted use of biomolecules in fluorescence imaging and Cerenkov luminescence for guided intraoperative imaging. Bacs' capacity for chelation provides opportunities for use in non-invasive positron emission tomography/computed tomography. Herein, we report the labeling of bacs with Hs1a, a (NaV1.7)-sodium-channel-binding peptide derived from the Chinese tarantula *Cyriopagopus schmidti* to yield Bac-Hs1a and radiolabeled Hs1a, which shuttles our bac sensor(s) to mouse nerves. In vivo, the bac sensor allowed us to observe high signal-to-background ratios in the nerves of animals injected with fluorescent Bac-Hs1a and radiolabeled Hs1a in all imaging modes. This study demonstrates that Bac-Hs1a and [^{64}Cu]Cu-Bac-Hs1a accumulate in peripheral nerves, providing contrast and utility in the preclinical space. For the chemistry and bio-imaging fields, this study represents an exciting starting point for the modular manipulation of bacs, their development and use as probes for diagnosis, and their deployment as formidable multiplex nerve-imaging agents for use in routine imaging experiments.

Graphical Abstract

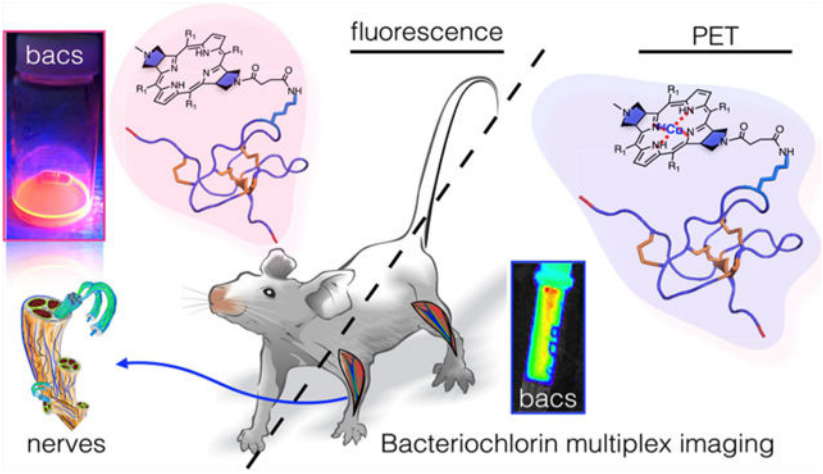

Bacteriochlorin are sensors with the intrinsic ability to be used in multiplex imaging, including fluorescence, Cerenkov Luminescence and PET, for surgery, non-invasively. These molecules have the tremendous potential to be employed in intraoperative imaging, providing *in vivo* guidance and rendering a quantification method.

INTRODUCTION

The use of porphyrinoid compounds as tracers is challenging, mainly due to their aromaticity, hydrophobicity, lack of amenable linkers, and scarcity.[1,2] To the best of our knowledge, clinically relevant red-absorbing and/or near-infrared dyes cannot be used to chelate metal ions or radionuclides, and most extant chelators are not fluorescent. Intuitively, an optical agent or tool offering such features, when added to a targeting vector, would represent an ideal bio-imaging agent for the much-needed quantitative assessment of cell

mechanism/distributions and the monitoring of changes in healthy and diseased tissue, generating rapid feedback or readouts of urgent medical conditions.[3] The ideal combination of a targeting molecule, a chelator, a radionuclide, and a conjugation method will yield a formidable radiotracer. The linker must also be carefully chosen, however, as activated esters increase the reactivity of the carboxylic acid; still, other click chemistry moieties are also effective, including amines, azides, propargyls, and octynes.[4]

Multiplex agents offer physiochemical benefits: such modular constructs can minimize differences that may occur in uptake, specificity, and biodistribution. We aim to develop porphyrins into bacteriochlorins in order to address the lack of modular multiplex constructs and to provide a quantitative imaging tool for use in the preclinical space. Although bacteriochlorins present superior chemo-photophysical properties for exploration as an optical tracer,[5] they have not been widely adopted by the imaging field.[6,7] Several in situ challenges have prevented their use as tracers in the trials and the clinic.[8] So far, most research has focused on bacteriochlorins' energy transfer, incorporation of isotopic atoms,[9] and light harvesting, leaving their practical electromagnetic properties[10] and imaging attributes understudied.[11] There has been no strategic development of bacteriochlorins for use in the bio-imaging field: after Woodward[12] first described their synthesis, research for in vivo use has been markedly slow. Inconveniently, past methods for the synthesis of bacteriochlorins have been proven difficult to carry out and resulted in low yields and purities.[7,13,14]

For the development of radiolabeled agents, the radiochemistry needs to be stable and reproducible to produce unperturbed physiochemical-active tracers. Our radiochemistry provides the following advantageous features that could be readily adapted to other platforms/constructs for the study of other medical afflictions following the same principles. If the researcher chooses the bioactive targeting molecule, then the use of a ligand, such as ethylenediaminetetraacetic acid (EDTA), hydroxypyridinone (HOPO), dodecane tetraacetic acid (DOTA), and a bacteriochlorin, coupled to the ideal radionuclide, could yield an excellent radiotracer for in vivo imaging[4] to effectively deliver payloads to the targeted area.[15] This collection of factors allows successful radiochemistry, providing an imaging window for research and interrogation depending on the nature of the study and radionuclide; in this case, copper-64 ($t_{1/2}$ = 12.7 h) provides a sufficient imaging window for our synthesis and experiments. This protocol most likely assures transforming the optical agent(s) into an amenable radiotracer.[15,16]

Here, aromatic porphyrins were transformed into bacteriochlorin sensors to facilitate in vivo nerve tissue imaging. Bacteriochlorins interconnected by pyrroles are near-infrared dyes absorbed at 700–735 nm and emitted at 740–760 nm—photophysical properties making them superior imaging molecules over other porphyrinoids.[7,17] Surprisingly, however, their ability to chelate metal ions and radionuclides has been underutilized, despite obvious advantages over other dyes/chelators that lack tandem chelation/fluorescence features. Conveniently, bacteriochlorins possess enhanced bio-optical properties compared with their sister chlorins and parent porphyrins, which are suitable for red-fluorescence imaging only and are limited to metalations, respectively.[18] Previous metalations of porphyrin[19] have been limited to the parent porphyrin core and phthalocyanines.[19] In porphyrins, the use of

metals, including copper-64,[20] has produced ambiguous results.[21] Labeling porphyrins with copper-64 for use in cancer patients yielded disappointing results,[21] but when a porphyrin antibody was labeled with copper-67, the results were more encouraging, showing tumor delineation.[22] Thus, conjugates of bacteriochlorins with a cell/tissue targeting moiety should be ideal in vivo imaging agents for use in the clinic.[16]

While multistep synthesis of bacteriochlorins was performed by the Lindsey group,[9,13,23] and enhanced, photostable, and soluble porphyrinoid derivatives were developed by the groups of Drain and Tome (Scheme S1A, S1B), no clinical evaluations have been reported.[14,24,25] In 2008, Foster and colleagues reported the use of a chlorin agent, NPe6, for the fluorescent visualization of breast cancer cells/tumors; they demonstrated rapid chlorin accumulation in the vasculature and extra-vasculature, generating some contrast between the tumor and surrounding tissue in vivo.[26,27] In 2011, Takashi and co-workers reported a chlorin-sugar conjugate for the detection and therapy of gastric and colon cancers, but no biomarker was presented for targeting.[28] In 2021, Spingler and colleagues reported the use of bacteriochlorins with anticancer activities in cervical cancer cells.[29] Pandey and Bruckner among others have used bacteriochlorins for imaging squamous cell carcinoma in vitro,[29] and two recent reviews[30,31] provide an overview of the field.[30,32]

NaV1.7, one of the nine subtypes of the human voltage-gated sodium channel, is recognized as an important biomarker for analgesic drugs.[33] NaV1.7 is highly expressed in peripheral nerves, including the dorsal root ganglia.[34] As a proof of principle for the use of bacteriochlorins as sensors, we attached them to Hs1a,[35,36] a peptide from the venom of the Chinese tarantula *Cyriopagopus schmidti*, which has high affinity for NaV1.7.[33,36] We envisioned that Hs1a could be efficiently labeled with the bacteriochlorin without affecting its physiochemical properties[25,37,38] and that the resulting Bac-Hs1a would be of clinical interest.[38,39] Both experimental and clinical data point toward better functional outcomes when an injured nerve is promptly repaired and/or reconstructed immediately.[40,41] The multimodal imaging functionality of radiolabeled Bac-Hs1a would allow non-invasive diagnosis of nerve damage by positron emission tomography/computed tomography (PET/CT) or PET/MRI imaging. The fluorescence of the bio-conjugate would also allow intraoperative identification of damaged nerves during surgical interventions, thus lending urgently needed intraoperative tools to operating surgeons.

Our bacteriochlorin synthetic method—reported here for the first time—uses a combined formal cycloaddition and an aromatic reaction to generate an asymmetric bacteriochlorin (Scheme 1). In brief, we inserted a pyrrolidine ring in the porphyrin core with the help of an amenable, still dynamic azomethine ylide (Y1) that generates a hydride and an inductive prolonged resonance due to the solvent effect. We tried to synthesize bacteriochlorins with the same Y1 ylide in chlorobenzene at 120 °C, but no bacteriochlorin was formed, suggesting that they do not follow the same cycloaddition mechanism.[8] This controllable desymmetrizing formal cycloaddition reaction produces a bacteriochlorin of interest and results in one pyrrolidine ring containing a methyl group, while the second pyrrolidine ring features a peripheral secondary amine, used as an anchor to append a carboxylate linker through which the bacteriochlorin was attached to Hs1a to yield Bac-Hs1a.[25] Furthermore, the Bac-Hs1a tetrapyrrole system allowed for radiolabeling with ^{64}Cu to yield

the radiotracer [^{64}Cu]Cu-Bac-Hs1a, suitable for Cerenkov luminescence and PET imaging of mouse peripheral nerves in vivo. The Bac-Hs1a conjugate is a powerful quantitative imaging tool capable of shuttling to inaccessible biomarkers with contemporaneous and rapid mesoscopic assessment using multi-imaging, Cerenkov luminescence, fluorescence, and PET modalities.

RESULTS

Synthetic bacteriochlorins were prepared via a formal cycloaddition and an aromatic reaction for multiplex imaging and engineered with exquisite and superior optical properties. The carboxylate linkers on the bacteriochlorins equate them to the standard of care FDA-approved dyes,[42] alongside their enhanced physiochemical stabilities, high solubility, excellent fluorescent brightness, narrow emission bands (10–25 nm), and chelation ability. Substantially, our synthetic bac's approach differs from the chlorin synthesis, as the formal one is suitable for true dipolar cycloaddition, as it occurs at one double bond only. Our porphyrinoids and synthetic route eliminate the promiscuous biodistributions and physiochemical issues that have plagued previous studies/syntheses.[1,26] With a pure bacteriochlorin in hand, we leveraged the dye's absorption and emission for maximum fluorescence production and performed radiolabeling and intensive assessment of the bacteriochlorin as a ligand to dentate radionuclides, including ^{64}Cu, for in vivo experiments in mouse models. Here, we show how mouse nerves lighted up with bacteriochlorin sensors, which could help in the identification of small nerves surrounding tumors to avoid unintended nerve injuries during surgeries, rendering a tremendous in vivo imaging tool to improve surgical outcomes.

Synthesis of a Fluorescent Bacteriochlorin and Conjugate, Bac-FL and Bac-Hs1a.

High-yielding bacteriochlorins were synthesized via a formal dipolar cycloaddition and an aromatic substitution reaction in 2–3 steps with a gradient temperature under dielectric dimethylformamide (DMF) solvent inducement (Scheme 2A). The starting compounds were tetrakis-(pentafluorophenyl) porphyrin **1** ($TPPF_{20}$) and the dynamic ylide **Y1**; an adjustable chemical synthesis protocol was developed to afford compound **4** featuring two opposed pyrrolidine rings, one bearing a methyl substituent and the second having a secondary amine. The yields of **4** were <3 and 38% in chlorobenzene and DMF, respectively, after recycling and reacting, and the purities were at least 93% for compounds **4–6**. With the help of a base, the peripheral secondary amine of **4** reacted with succinic anhydride in dichloromethane, which afforded compound **5** in at least 10 min ($n = 6$). Compound **5** features a peripheral carboxylate linker, activated with *N*-hydroxysuccinimide to obtain a bacteriochlorin NHS-ester compound **6**, which can be appended to different targeting biomolecules to serve as an amenable sensor (Scheme 2B). To assess the properties of compound **6** (Bac-FL) (ex_{max} = 690–710 nm, em_{max} = 720–750 nm), the bacteriochlorin was used to label a 35-amino-acid sequence synthetic Hs1a peptide[36] via amide bond formation (Scheme 2C,D). The reaction was performed under basic conditions with a carbonate in a 1:1 solution of water and acetonitrile in the dark, yielding Bac-Hs1a in 20% yield and at least 94% purity. With Bac-Hs1a in hand, chelation to ^{64}Cu was carried out under acidic aqueous conditions at 37 °C for ~30 min to yield [^{64}Cu]Cu-Bac-Hs1a.

Chemical Characterization of Bac-FL, Bac-Hs1a, Site of Conjugation and Affinity.

Absorption spectra of **4–6** and Bac-Hs1a (Figures 1A and S1A) show the characteristic 725 nm absorption signal in functionalized bacteriochlorins; no other type of chromophore absorbance was observed in the farred range (Figure S1A). The fluorescence emission maxima were 730–732 nm for compounds **4–6** and Bac-Hs1a, consistent with previous results[7] (Figures 1B and S1B). Conveniently, fluorescence bands of Bac-FL and Bac-Hs1a overlapped with the peaks of compounds **5** and **6** but not for the Hs1a peptide alone (Figure 1B). The dye Bac-FL (**6**), the fluorescent Hs1a, and the radiolabeled Hs1a were synthesized successfully to demonstrate utility using different imagining modalities. In brief, compound **5** was isolated with 90% yield and 93% purity, and it had a retention time (t_R) of 18 min on an Atlantis T3 C18 RP-HLPC column (Figure S1C). Compound **6** had a retention time of 19 min using the same column, and it was isolated with 60% yield and 90% purity (Figure S1D). LC/MS spectra of compounds **5** and **6** (Bac-FL) showed clean ionic peak families, with observed monoisotopic masses at 1173.35 and 1270.06, respectively (Figure S1E). Compound **6** (Bac-FL) was used to label synthetic peptide Hs1a[35,36] under basic conditions to yield Bac-Hs1a in 20% yield and 96% purity. An HPLC chromatogram shows the retention time (t_R) increase from 20.0 min for Hs1a to 22.0 min for Bac-Hs1a (Figures 1C and S1F). LC/MS was used to confirm the expected masses of the peptides (3851.74 and 5007.01 Da for Hs1a and Bac-Hs1a, respectively; Figure 1D). For the absorption and emission spectra of Hs1a and Bac-Hs1a, the characteristic 720–732 nm peak for the bacteriochlorin family was used as a reference, and it was observed for Bac-Hs1a at 720 and 732 nm for absorption and emission, respectively (Figure 1B).

With tryptic digest experiments, we determined the location of the bacteriochlorin fluorophore site of conjugation. For the unmodified Hs1a, we found ions that correspond to the fragment G1-K17 (1865.80 Da, Figure S2A). Conveniently, this fragment was not observed for digested Bac-Hs1a; instead, the fluorescent Hs1a peptide produced a novel fragment G1-K17 plus the intact mass of the bacteriochlorin molecule (3023.96 Da, Figure S2B). This peak suggests that the likely conjugation occurred at K14; this predominant conjugation at K14 is likely electronically or sterically favored. In addition, we also observe a small amount of fluorescent side products, including Hs1a with two conjugated bacs, which were not further characterized.

We assessed the effect of Hs1a and Bac-Hs1a on human NaV1.7 using automated whole-cell patch-clamp electrophysiology. Hs1a is an exquisite potent inhibitor of NaV1.7 (IC_{50} = 35 nM), and its potency is only marginally reduced by addition of the bacteriochlorin to yield Bac-Hs1a (IC_{50} = 45 nM) (Figure 1E). We conclude that fluorescence modification of Hs1a slightly reduces its potency, but it remains a potent nanomolar inhibitor of NaV1.7 and a formidable agent for targeting peripheral neurons. Furthermore, additional physical–chemical characteristics are reported, including exclusive features of compounds **5** and **6** (Bac-FL) and Bac-Hs1a, comprising absorbance and emission maxima, quantum yields, intensity of Q bands, RP-HPLC retention times, and obtained yields, which are presented in Figure 1F.

In general, our synthesized bacteriochlorins exhibit the porphyrin core, and their identities were corroborated using ^{1}H and ^{13}C NMR (Spectra S1, S2) experiments, which followed reported patterns. Repeatedly, the ^{1}H NMR spectra of our synthetic bacteriochlorins show proton aromatic signals at around 8.38–8.72 ppm and proton nuclear magnetic resonance (NMR) signals at around 5.1 ppm for the β-pyrrole protons and at around 2.3 and 2.8 ppm for the methylene protons of the inserted pyrrolidine rings; the methyl protons for the peripheral pyrrolidine appear at 1.8 ppm. Depending on the linker or the type of the activator used, more resonances will appear in the aliphatic region, for instance, resonances at 2.6 and 3.1 ppm are detected for the carboxylate linker of compound **5**, alike resonances appear for compound **6** but extra resonances at the aliphatic region are observed due to the succinimide moiety.[25] ^{13}C NMR spectra showed a repeated pattern, clearly showing multiple resonances from the bacteriochlorin backbone, 8 resonances for the quaternary carbons of the bacteriochlorin core, 6 resonances for carbons attached to F-atoms, 2 aromatic resonances for the pyrroles, 4 aliphatic resonances for the inserted pyrrolidines, and 2 more quaternary carbons and 2 more aliphatic resonances that correspond to the carboxylate linker for compound **5**.

Design of a Targeted [^{64}Cu]Cu-Bac-Hs1a Radiotracer for In Vivo PET Imaging.

With the Hs1a-targeting construct in hand, we sought to explore its potential as a PET radiotracer. The presence of the phenyl substituents attached to the core of the bacteriochlorin increases the acidity of the central N-atoms and improves the rate and yield of metal insertion. We therefore tested whether Bac-Hs1a could efficiently chelate ^{64}Cu(II), as shown previously for a sister chlorin.[16] In brief, Bac-Hs1a was labeled with ^{64}Cu under acidic aqueous conditions (0.1 M NH_4OAc, pH 6) at 37 °C for ~30 min to yield [^{64}Cu]Cu-Bac-Hs1a (Figure 2A). The reaction was carried out with a radiochemical conversion rate of more than 70%. The product was obtained with >95% radiochemical purity and in 40–50% isolated radiochemical yield (n.d.c.), which corresponded to maximum molar activities of 0.1–0.2 GBq·μmol^{-1}. The reaction was monitored by instant thin-layer chromatography (iTLC), and the conjugate was purified using a C18 cartridge. Bac-Hs1a (observed at 280 nm) and [^{64}Cu]Cu-Bac-Hs1a had a similar t_R of 21 min on an Atlantis T3 C18 column (Figure 2B). Furthermore, stability experiments were performed on the newly prepared [^{64}Cu]Cu-Bac-Hs1a using a Radio-HPLC in saline and serum solutions, showing high stability of the radiolabeled tracer (Figure 2C).

The synthesis of [^{64}Cu]Cu-Bac-Hs1a was accomplished successfully and is reported here for the first time. In general, to develop an efficient nerve radiotracer, some issues must be considered: first, the ligand must have the ability to chelate ^{64}Cu by efficient dentation; second, the radiotracer construct must maintain the physiochemical properties of the Hs1a peptide to continue targeting nerve tissue after chemical modification/variation and/or formulation, including an in vivo experiment. Immediately after the radiochemical synthesis, phosphate-buffered saline (PBS), a block formulation (unlabeled Hs1a and radiotracer), and formulated [^{64}Cu]Cu-Bac-Hs1a were imaged using Cerenkov luminescence (Figure 2D).

In Vivo Performance of Bacteriochlorin Labeled Peptide, Bac-Hs1a.

Our previous work with sister chlorins provided evidence of the innate fluorescence of the chlorin porphyrinoid family. Figure 3A shows the workflow for assessing in vivo fluorescence-guided identification of nerves based on the Bac-Hs1a NaV1.7-targeting biomolecule, which shuttles to mouse peripheral nerves due to the high expression of NaV1.7. Under mesoscopic imaging conditions, we observed rapid and selective accumulation of Bac-Hs1a within the peripheral nerves of mice (Figures 3B and S3A, S3B). Athymic mice were injected intravenously with either Bac-Hs1a (1 nmol, 11 μM of Bac-Hs1a in 100 μL PBS) or 100 μL PBS and sacrificed 30 min later; all procedures were terminal. The peripheral nerves on the upper and lower extremities were exposed, and epifluorescence imaging was performed in vivo using an IVIS Spectrum (ex: 680/20 nm; em: 720–750 nm). In mice receiving just the imaging agent, the peripheral nerves were clearly visible, with high fluorescence from the bacteriochlorin sensor, whereas in mice receiving the PBS vehicle, fluorescence was low (brachial plexus, radiant efficiency: $0.5 \pm 0.3 \times 10^9$ and $0.01 \pm 0.02 \times 10^9$ for Bac-Hs1a and PBS, respectively, and sciatic nerve, radiant efficiency: $0.9 \pm 0.1 \times 10^9$ and $0.06 \pm 0.03 \times 10^9$ for Bac-Hs1a and PBS, respectively, Student's unpaired *t* test, $^{**}P < 0.01$, $^{****}P < 0.0001$, NS, not significant, Figures 3B,C and S3B).

We found no difference in the radiant efficiency between the before surgical nerve exposure and after surgical nerve exposure in mice after the lateral tail vein injection (pre- and post-radiant efficiency: $0.7 \pm 0.04 \times 10^9$ and $0.69 \pm 0.02 \times 10^9$, respectively). When comparing the radiant efficiency of animals injected with the fluorescent contrast agent and PBS, we found a statistically significant difference of 44-fold in the brachial plexus and a difference of 15-fold in the sciatic nerve, as well as a 20-fold difference between the groups injected with Bac-Hs1a and PBS when considering all exposed nerves (upper and lower body nerves). For the biodistribution experiments, we have observed a clear trend toward fluorescence in the kidneys and livers of animals injected with the imaging agent only (kidney radiant efficiency: $3.8 \pm 1.3 \times 10^7$ and liver radiant efficiency: $2.1 \pm 1.0 \times 10^7$) and for those kidneys and livers injected with PBS (kidney radiant efficiency: $0.6 \pm 0.02 \times 10^7$ and liver radiant efficiency: $0.6 \pm 0.06 \times 10^7$). In these experiments, we did not observe significant fluorescence in any other organ, including the muscles, heart, spleen, and brain, when we compared animal groups injected with Bac-Hs1a and PBS (Figure 3D).

Confocal Microscopy of Bac-Hs1a.

Resected sciatic nerves of animals injected with Bac-Hs1a (1 nmol, 10 μM Bac-Hs1a in 100 μL of PBS) or PBS were microscopically imaged to show elongated nerve topography; these rope-like structures are Schwann cells populating peripheral nerves, which corroborates previous observations from our group.[38] For these fresh tissue staining experiments, resected mouse nerves were counterstained with Hoechst 33342 (blue, 20 μM, 1 nmol in 50 μL of PBS) and placed directly on a microscope slide for the corresponding fluorescence imaging (Figures 3E and S4). Adjacent H&E and anti-NaV1.7 staining validated fluorescence microscopy structures observed with Bac-Hs1a, resembling tubular nerve bundles.

Cerenkov Luminescence of [^{64}Cu]Cu-Bac-Hs1a.

For [^{64}Cu]Cu-Bac-Hs1a, the uptake specificity on peripheral nerves on the upper and lower body was striking (Figures 4A and S5). In mice receiving the imaging agent alone (3.1–4.1 MBq in 150 μL of PBS), the brachial plexus and sciatic nerves were clearly detected, with a mean radiant efficiency of 6543 ± 2008 p/s/cm^2/sr (Figures 4A–C and S61A, B), whereas the "blocking" group (mice receiving the imaging agent in combination with the unmodified Hs1a peptide, 21 nmol, 210 μM in 100 μL of PBS) had a statistically significant lower accumulation (Student's unpaired *t* test, $P < 0.0001$, 43-fold reduced 746 ± 152 radiant efficiency).

When analyzing the nerves ex vivo, high Cerenkov luminescence was observed on the peripheral nerves of animals injected with [^{64}Cu]Cu-Bac-Hs1a (Figure S6A). We found a mean radiant efficiency of 6378 ± 2048 for the brachial plexus and a radiant efficiency of 6635 ± 1773 for the sciatic nerves, whereas in animals receiving a block formulation, less luminescence signal was observed, 680 ± 64 for the brachial plexus and 765 ± 117 for the sciatic nerve (Figure S6B). In these sets of experiments, the sites of off-target uptake ex vivo appear to be the liver, spleen, and kidney (Figure 4C). No uptake was evident in other organs, including the muscles, heart, and brain, for animals injected with the combination of [^{64}Cu]Cu-Bac-Hs1a and unmodified Hs1a (Figure 4C), using region of interest (ROIs) that were drawn on all resected organs under overlay guidance.

Additionally, to assess acute biodistribution, radioactivity associated with each organ was expressed as a percentage of injected dose per gram of tissue (% ID/g). This quantitative measurement showed uptake on peripheral nerves, liver, and spleen (41.8 ± 0.8, 35.8 ± 0.5, and 978 ± 1.2 %ID/g, respectively; Figure S6C). Uptake in the spleen and kidneys in the gamma counter is caused by measurable Cerenkov radiations when they enter the tissue in the dark.[43]

Pharmacokinetics of the [^{64}Cu]Cu-Bac-Hs1a Radiotracer.

Next, we investigated the potential of the radioactive tracer as a tool for delineating mouse nerves in vivo (Figures 5A and S7–S10). Athymic nude mice (6–8 weeks) were injected with [^{64}Cu]Cu-Bac-Hs1a (300–350 μCi, 11.1–13.0 MBq, 0.66–0.77 nmol). Static PET scans were subsequently acquired 30 min after the administration of the radiotracer (Figures 5A, S7, and S8). As early as 30 min post-injection, nerves were clearly delineated. Peripheral nerves were the only tissue that displayed high uptake of the injected radiotracer with a low background signal remaining in the rest of the healthy organs, apart from the liver and spleen, and the corresponding organs of the block formulation group.

In addition, static PET scans were taken from the resected nerves. Significant nerve uptake was also observed (Figures 5B and S11). An acute biodistribution experiment was performed to more accurately quantify the in vivo biodistribution. Significant nerve uptake was observed in situ 60 min post-injection (38.5 ± 9.8 and 39.2 ± 1.4 %ID/g) when nerves were completely resected. Low levels of uptake were observed in the heart (0.7 ± 1.2 %ID/g), muscle (0.2 ± 1.4 %ID/g), kidney (1.8 ± 1.7 %ID/g), and spleen (0.7 ± 1.2 %ID/g, Figure 5C). The liver showed the highest non-target uptake (9.8 ± 2.8 % ID/g) at

60 min post-injection, an observation consistent with our observed Cerenkov luminescence experiments. For the block formulation, the liver showed the highest non-target uptake (19.6 ± 1.9 %ID/g) at 60 min post-injection.

DISCUSSION

Using our chemical protocol, we synthesized bacteriochlorins via formal cycloaddition and successfully leveraged their multiplex properties. These light-driven systems generated exciting results, providing true near-infrared fluorescence and, with their tetrapyrrole system, chelating the radiometal ^{64}Cu for use as a formidable radiotracer. In addition, as demonstrated by our chemical characterization, multimodal nerve imaging, and in vivo experiments, quantifiable bacteriochlorin sensors were formed and delivered; we expect these sensors to significantly impact the imaging and chemical fields, especially with regard to porphyrin development.

Our bacteriochlorins result from a trimolecular reaction involving mechanism(s) that afford asymmetry via formal cycloaddition. While it is true that our bacteriochlorin synthesis was inspired by the synthesis of Tome/Drain[7,14] and colleagues, our synthesis uses a different route to yield bacteriochlorins. In the past, we have explored chlorin syntheses and found that the sister chlorin uses dipolar cycloaddition for its exclusive synthesis.[8,37] In this past chemical endeavor, we have tested different conditions and temperatures and have changed reaction times and used chlorobenzene/toluene.[25,37] These chemical manipulations did not yield a bacteriochlorin of interest (Scheme S1), only very small amounts of bacteriochlorin were detected by LC–MS.[37] Our bacteriochlorin reaction is a formal cycloaddition beginning with the formation of the used but understudied ylide **Y1**, which forms/reacts via a disproportionation reaction, yielding a type of sister chlorin (see Scheme 1). Conveniently, this newly synthesized chlorin (a reduced porphyrin) could take the form of an intermediate imine chlorin cation; under the influence of a refluxing high dielectric solvent such as polar DMF, this form allows for charged molecules and hydride formation and retention. The solvent effect induces a prolonged aromatic resonance that activates a double bond at positions 7 and 8 of the newly prepared porphyrinoid, which favorably reacts with a second **Y1** to close pyrrolidine ring A so that the resonance effect continues throughout π-conjugation and closes pyrrolidine ring B, which finally affords a bac of interest, before deformylation and dehydration yield asymmetric bacteriochlorin **4**. This mechanism and observation are also sustained by the crucial monitoring/reaction of chlorin and **Y1** under chlorobenzene at 120–130 °C, where no bacteriochlorin was formed, and its detection was not possible with gravity chromatography methods and HPLC. This reaction rules out the possibility of bacteriochlorin formation via dipolar cycloaddition using a double bond of a chlorin.

Past attempts to synthesize chlorins, often performed with lower-grade dielectric solvents, including chlorobenzene/toluene, suffered from limited resonance, which in turn limits the reactivity of the double bond on the chlorin and the potential formation of the bacteriochlorin.[37,44,45] This observation is supported by the lack of bacteriochlorin formation; even when utilizing other ylides such as sarcosine for dipolar cycloaddition, this route leads to unclickable chlorins.[14] In contrast, the use of a high-grade dielectric solvent

induces a trimolecular reaction via resonance, increases the reactivity of the double bond for a continued resonance effect, and allows for the insertion of the two pyrrolidine rings required in bacteriochlorins. Generally, a trimolecular reaction is rare, but our proposed mechanism and results explain the formation of bacteriochlorins in DMF. Again, a crucial validation of this finding can be seen in the lack of bacteriochlorin formation after purified chlorin was reacted with **Y1** in chlorobenzene, a reaction tested as well by the Cavaleiro group (years 1999–2008),[45] producing the same results.[14,44]

In recent years, significant efforts have been made to develop in vivo tracers that can identify malignant tumors.[46] Identifying the small nerves surrounding those tumors is also of utmost importance when considering post-operative functional outcomes. Currently, small nerve identification relies heavily on visual observation, tactual exploration by the surgeon, and subjective patient feedback.[36,47] No molecular tools are available for immediate and precise assessment of at-risk vital nerves,[48] which, once damaged, might negatively impact a patient's quality of life.[49]

In 2019, we reported a proof-of-principle tracer for in vivo labeling of the peripheral nervous system in mice,[38] but a near-infrared multimodal nerve imaging agent has not yet been reported. Such an agent would be clinically useful insofar as it would allow physicians to rapidly assess the magnitude of potential nerve trauma: PET/CT could provide rapid assessment of nerve damage using the radiolabeled part of the conjugate. In the cases requiring surgical intervention, the fluorescent (or Cerenkov luminescence light) properties of the same compound would allow nerve identification and facilitate surgical repair, preventing further deterioration of the damaged nerve structures.[16,39,40]

In line with our previous experience with the Hs1a peptide and porphyrinoids, we set about devising a reproducible strategy that would proceed via modification of a lysine residue, which ultimately would take the form of an amide bond formation.[38] In this work, we selected bacteriochlorin **6** for labeling and chelation. A bacteriochlorin is a known fluorophore and the best representative of the porphyrin family,[8] allowing for in vivo monitoring and signal quantification using fluorescence, Cerenkov luminescence, or PET.[33]

Labeling of a bacteriochlorin carboxylate to Hs1a was successfully carried out, and absorbance and fluorescence spectra of Bac-Hs1a demonstrated that labeling did not interfere with the photophysical properties of the peptide or the bacteriochlorin as no other chromophoric signals at 730 nm were observed and the Bac-Hs1a conjugate retained its affinity for channel NaV1.7, as demonstrated by our in vitro work. When injected into nude mice, Bac-Hs1a showed high uptake in peripheral nerves after 30 min, as confirmed by IVIS imaging and ex vivo biodistribution. Specific uptake of Bac-Hs1a was confirmed using an excess of the unlabeled Hs1a peptide. In so doing, this confirmed that the bacteriochlorin tether did not significantly perturb the binding of Hs1a to its molecular target, NaV1.7.

We then radiolabeled Bac-Hs1a and evaluated it in mice in vivo. While fluorescence experiments confirmed our previous work with sisters chlorins, the exciting aspect comes from the non-invasive accumulation of radiolabeled Hs1a in nerves. Similar to Bac-Hs1a, [^{64}Cu]Cu-Bac-Hs1a showed high specific uptake on peripheral nerves in our PET/CT

images. In vivo, the radiotracer uptake was semi-quantified via the use of Cerenkov luminescence and PET. This was accompanied by ex vivo analysis of resected nerves and the key mouse organs. We have demonstrated that Cerenkov luminescence and PET using nerve-targeting agents coupled to enhanced optical molecules such as bacteriochlorins may serve as a powerful alternative to whole-body in vivo imaging of the peripheral nervous system.

After demonstrating that bacteriochlorins can be used to label peptides and that the constructs can be effectively shuttled to peripheral nerves, it is worth mentioning other benefits of the Bac-Hs1a radiotracer, especially as regards Cerenkov luminescence. For instance, in developing countries, the use of Cerenkov luminescence can be an effective alternative to PET due to the adaptability of the Cerenkov luminescence cameras and the variety of inexpensive, compatible radioisotopes that are available, which reduces the cost of this technology compared to PET. The development of bacteriochlorin-based tracers sets Cerenkov luminescence on a good trajectory for affordable nuclear imaging, encouraging the sharing of in vivo-guided imaging/technology with researchers and physicians around the world.

CONCLUSIONS

Our novel synthetic method yielded bacteriochlorin(s) designed for use as quantitative tools in preclinical and clinical imaging. We show that bacteriochlorins, formed by formal cycloaddition, are ideal optical sensors, superior to existing near-infrared dyes and chelators due to their suitability for both fluorescence and PET. While bacteriochlorins coupled to bioactive targeting peptides such as Hs1a proved to be useful chemical sensors for in vivo nerve imaging, other targets or tissue could also be reliably quantified with bacteriochlorins. Both Bac-Hs1a and [^{64}Cu]Cu-Bac-Hs1a tracers accumulated in peripheral nerves with striking success. We believe this approach, combining fluorescence, Cerenkov luminescence, and PET, could shift paradigms in the use of bacteriochlorins for intraoperative imaging of the peripheral nervous system. Both Bac-Hs1a and [^{64}Cu]Cu-Bac-Hs1a are promising tools whose translation could help physicians rapidly identify lesions and act immediately to preserve or reconstruct vital nerves in order to avoid catastrophic nerve damage. Bacteriochlorins, with their multiplex properties, have proven to be formidable in vivo sensors, adaptable constructs across different imaging modalities, and potential tools to measure disease progression when conjugated to a targeting molecule.

EXPERIMENTAL METHODS

Unless otherwise indicated, all solvents and reagents were obtained from Sigma-Aldrich or Fisher Scientific and used without further purification. Fluorescently labeled and radiolabeled Hs1a were prepared following our previous reports.[7,14,25] Acetonitrile (ACN) and water (H_2O) were the most used solvents and were graded for high-performance liquid chromatography (HPLC) and liquid chromatography–mass spectroscopy (LCMS) in order to perform standard chemical validation experiments. PBS without Ca^{2+} or Mg^{2+} was obtained either from MSK media facility or was commercially obtained from Fisher and used for compound formulations and all in vivo injections.

Chemical Synthesis of Bacteriochlorins.

In general, for the repeatable synthesis of bacteriochlorins, 5,10,15,20-tetrakis-(2,3,4,5,6-pentafluorophenyl)-porphyrin $TPPF_{20}$ (100 mg, 0.102 mmol) was dissolved in 10 mL of *N*,*N*-dimethylformamide (DMF) and reacted with dynamic ylide **Y1** previously prepared by grinding a mixture of glycine (770 mg, 10.05 mmol) and paraformaldehyde (300.8 mg, 10.05 mmol). The prepared ylide **Y1** was added in 10 aliquots (100 mg of ylide on each addition) every 30 min and allowed to react at 150–152 °C, under a N_2 atmosphere for 5 h; the reaction temperature was increased to 170 °C, and extra 10 aliquots of ylide Y1 were added every 30 min to the reaction mixture after 5 h, and the reaction was allowed to continue overnight. DMF was evaporated with the help of a lyophilizer. The crude mixture was dissolved in ACN for HLPC purification to afford **4** as a reddish powder, 38% yield. Compound **4** (50 mg, 0.047 mmol) was dissolved in 6 mL of CH_2Cl_2, and 50 μL of NEt_3 (40 μmol) was added to the reaction mixture. Succinic anhydride (48 mg, 0.48 mmol) was added to the same reaction mixture, which was allowed to proceed for 45 min to afford **5**, 90% yield, which was purified by HPLC. To compound **5** (5 mg, 4.3 nmol) dissolved in 6 mL of tetrahydrofuran (THF), *N*-hydroxysuccinimide (5 mg, 0.04 mmol) and dicyclohexylcarbodiimide (DCC, 9.9 mg, 0.05 mmol) were added inside a 10 mL vial to start the reaction, which was allowed to react at room temperature (r.t.) for 30 min; the product, **6**, was filtered and HPLC-purified; the yield was 40%. For compound **5**, ^{1}H NMR (500 MHz, CDCl3) δ 8.72 (d, J = 4.85 Hz, 2H), 8.38–8.49 (m, 2H), 5.22–5.28 (m, 4H), 3.17 (t, J = 10.15 Hz, 1H), 2.64 (t, J = 9.95 Hz, 1H), 2.38–2.41 (m, 2H), 2.18–2.21 (m, 4H), 1.63–1.68 (m, 4H), 1.61 (s, 3H), −1.82 (s, 2H); ^{13}C NMR (125 MHz, CDCl3) δ; 168.75, 168.68, 152.73, 147.49, 147.29, 145.57, 145.27, 143.16, 141.08, 140.32, 138.51, 136.51, 135.26, 132.40, 128.07, 123.90, 119.39, 116.59, 106.21, 96.71, 60.50, 52.82, 52.26, 28.16, 24.14, 14.85. LC–MS (ESI) m/z calcd for $C_{53}H_{26}F_{20}N_6O_3$ ($[M-H]^-$), 1174.1747, found 1173.3538. For compound 6, LC–MS (ESI) m/z calcd for $C_{57}H_{29}F_{20}N_7O_3$ ($[M-H]^-$), 1271.1061, found 1170.0648.

Synthesis of Hs1a.

As previously reported by our team,[50] Hs1a was prepared and oxidized on a CEM Liberty Prime microwave peptide synthesizer (CEM corporation, NC, USA) on Rink-amide polystyrene resin to the synthetic peptide.[51] The Hs1a peptide was simultaneously released from the resin, and the side chain protecting groups were removed using trifluoroacetic acid (TFA)/triisopropylsilane (TIPS)/water (48:1:1 v/v/v) for 2.5 h. After trituration in chilled diethyl ether (Et_2O) of the crude Hs1a, the precipitated peptide was subjected to separation using solvent A/B (45% v/v ACN, 0.05% v/v TFA), lyophilized, and then pre-purified using C18 RP-HPLC. The pure peptide was eluted using a linear gradient of 10–60% solvent B (90% v/v ACN; 0.05% v/v TFA) over 50 min with a flow rate of 8 mL·min^{-1}. Oxidation of free cysteines took place at room temperature for 16 h in a buffer containing 2 M urea, 0.1 M Tris pH 8, 0.15 mM reduced glutathione, and 0.3 mM oxidized glutathione. A single sharp peak was obtained from the final analytical RP-HPLC purification, and 96% purity was achieved as calculated from the area under the curve. LC-ESI-MS (ES+), m/z calculated for the Hs1a peptide, $[C_{164}H_{251}N_{49}O_{47}S_6]$ 3851.74, $[C_{164}H_{251}N_{49}O_{47}S_6 + 2H]^{2+}$

1926.88, found $[M + 2H]^{2+}$ 1927.72, $[C_{164}H_{251}N_{49}O_{47}S_6 + 3H]^{3+}$ 1284.92, found $[M + 3H]^{3+}$ 1285.75, $[C_{164}H_{251}N_{49}O_{47}S_6 + 4H]^{4+}$ 963.94, found $[M + 4H]^{4+}$ 964.85.

Labeling of Bacteriochlorin to Hs1a Peptide, Bac-Hs1a.

Next, we looked forward to the appending of the bacteriochlorin dye to the Hs1a peptide via nucleophilic substitution, analogous to our previous work with similarly sized bioactive peptides.[52] In brief, the newly prepared bacteriochlorin-NHS ester, Bac-FL (0.67 mM, 85 μg in 100 μL of ACN), was added dropwise to the Hs1a peptide (0.65 mM, 250 μg in 200 μL of ACN) contained in a solution of Na_2CO_3 (1 M, 50 μL) to perform the required labeling which was allowed to occur for at least 10 min, followed by quick verification via HPLC. The product, Bac-Hs1a, was purified using RP-HPLC, and then, LCMS was performed. The excess solvent was removed in vacuo, yielding Bac-Hs1a as a reddish powder (50 μg, 20% isolated yield). Final analysis of the RP-HPLC purification showed 96% purity, using an RP-HLPC column (Atlantis T3 C18) with a gradient of 0–95% B over 40 min (A: H_2O/0.1%TFA, B: 99.9% ACN/0.1% TFA). LC-ESI-MS (ES+), m/z calculated for Bac-Hs1a, $[C_{218}H_{278}F_{20}N_{55}O_{49}S_6]$ 5006.94, $[C_{218}H_{278}F_{20}N_{55}O_{49}S_6 + 3H]^{3+}$ 1669.98, found $[M + 3H]^{3+}$ 1671.10, $[C_{218}H_{278}F_{20}N_{55}O_{49}S_6 + 4H]^{4+}$ 1252.74, found $[M + 4H]^{4+}$ 1253.53.

Synthesis of [^{64}Cu]Cu-Bac-Hs1a.

Radiolabeling of Bac-Hs1a (0.20 mM, 50 μg in 50 μL of 1:1 H_2O/DMSO) was performed using 3.8 μL of ^{64}Cu (111 MBq) in 500 μL of ammonium acetate buffer for 30 min at 37 °C. The [^{64}Cu]Cu-Bac-Hs1a was trapped on a preconditioned C18 cartridge (ethanol/water), washed with H_2O to remove free copper-64, and then eluted with ethanol to obtain pure [^{64}Cu]Cu-Bac-Hs1a. The specific activity of [^{64}Cu]Cu-Bac-Hs1a throughout the study was measured to be between 4.52 and 9.51 MBq/μg. [^{64}Cu]Cu-Bac-Hs1a was used for characterization and was formulated in PBS for in vivo studies with athymic nude mice.

iTLC Quantification.

The crude reaction mixture and purified labeled Hs1a peptide solution were analyzed by iTLC (glass microfiber chromatography paper impregnated with silica gel, 100 10 mm) using 50 mM EDTA (pH 5.5) as the mobile phase. For the control, [^{64}Cu]$CuCl_2$ (approx. 0.074 MBq) was mixed with ammonium acetate (0.1 M, pH 6.0) and incubated for 30 min at 37 °C. The same mobile phase was used for separation. The different iTLC plates were analyzed by iTLC and Laura 3 software (LabLogic, Sheffield, UK). [^{64}Cu]$CuCl_2$ R_f = 0.68–0.78; [^{64}Cu]Cu-Bac-Hs1a R_f = 0.28–0.31.

Statistical Analyses.

Statistical analyses were performed using GraphPad Prism 9. Unless otherwise stated, data points represent mean values, and error bars represent standard deviations of biological replicates. P values were calculated using Student's unpaired t test.

Supplementary Material

Refer to Web version on PubMed Central for supplementary material.

ACKNOWLEDGMENTS

The authors thank Professor Shengping Zheng from the Chemistry Department of Hunter College (CUNY) for his immensely helpful discussion about the mechanism of bacteriochlorin formation involving solvent effects and formal cycloaddition. The authors thank the Imaging and Radiation Sciences Program and the MSK Molecularly Targeted Intraoperative Imaging Fund, the Small Animal Imaging Core (P. Zanzonico, V. Longo), the Radiochemistry and Molecular Imaging Probes Core (S. Lyashchenko), and the Molecular Cytology Core at Memorial Sloan Kettering Cancer Center for support. The authors also thank Dr. Snehal Patel and Dr. Ian Ganly for help in nerve dissection. The funding sources were not involved in study design, data collection and analysis, writing of the report, or the decision to submit this article for publication. All authors carefully read and edited the manuscript. J.H.-G. thanks the support of the “Maria Zambrano” Program of Excellence within the framework of grants for talent retaining of the Universitat Politecnica de Valencia and the Spanish Ministry of Universities, funded by the European Union-Next Generation (UPV Contract C16684).

Funding

This work was supported by the National Institutes of Health grants R00 GM145587, R01 EB029769, R35CA232130, and P30 CA008748, grant agreement no. 796672, the Australian National Health and Medical Research Council (Project Grant APP1080405, Program Grant APP1072113 to G.F.K.), and the Australian Research Council (Centre of Excellence grant CE200100012 to G.F.K.).

REFERENCES

(1). Escobedo JO; Rusin O; Lim S; Strongin RM NIR dyes for bioimaging applications. Curr. Opin. Chem. Biol. 2010, 14, 64–70. [PubMed: 19926332]

(2). Luo S; Zhang E; Su Y; Cheng T; Shi C A review of NIR dyes in cancer targeting and imaging. Biomaterials 2011, 32, 7127–7138. [PubMed: 21724249]

(3). Rao J; Dragulescu-Andrasi A; Yao H Fluorescence imaging in vivo: recent advances. Curr. Opin. Biotechnol. 2007, 18, 17–25. [PubMed: 17234399]

(4). Zeng D; Zeglis BM; Lewis JS; Anderson CJ The growing impact of bioorthogonal click chemistry on the development of radiopharmaceuticals. J. Nucl. Med. 2013, 54, 829–832. [PubMed: 23616581]

(5). Ogata F; Nagaya T; Maruoka Y; Akhigbe J; Meares A; Lucero MY; Satraitis A; Fujimura D; Okada R; Inagaki F; et al. Activatable Near-Infrared Fluorescence Imaging Using PEGylated Bacteriochlorin-Based Chlorin and BODIPY-Dyads as Probes for Detecting Cancer. Bioconjugate Chem. 2019, 30, 169–183.

(6). Hong G; Antaris AL; Dai H Near-infrared fluorophores for biomedical imaging. Nat. Biomed. Eng. 2017, 1, No. 0010.

(7). Singh S; Aggarwal A; Thompson S; Tome JP; Zhu X; Samaroo D; Vinodu M; Gao R; Drain CM Synthesis and photophysical properties of thioglycosylated chlorins, isobacteriochlorins, and bacteriochlorins for bioimaging and diagnostics. Bioconjugate Chem. 2010, 21, 2136–2146.

(8). Hernandez-Gil J; Lewis JS; Reiner T; Drain CM; Gonzales J Leveraging synthetic chlorins for bio-imaging applications. Chem. Commun. 2020, 56, 12608–12611.

(9). Jing H; Tang Q; Bocian DF; Lindsey JS De Novo Synthesis of Bacteriochlorins Bearing Four Trideuteriomethyl Groups. Organics 2022, 3, 22–37.

(10). Battersby AR Tetrapyrroles: the pigments of life. Nat. Prod. Rep. 2000, 17, 507–526. [PubMed: 11152419]

(11). Vicente MD; Smith KM Syntheses and Functionalizations of Porphyrin Macrocycles. Curr. Org. Synth. 2014, 11, 3–28. [PubMed: 25484638]

(12). Woodward RB Total synthese des Chlorophylls. Angew. Chem. 1960, 72, 651–662.

(13). Lindsey JS De novo synthesis of gem-dialkyl chlorophyll analogues for probing and emulating our green world. Chem. Rev. 2015, 115, 6534–6620. [PubMed: 26068531]

(14). Silva AM; Tome AC; Neves MG; Silva AM; Cavaleiro JA 1,3-dipolar cycloaddition reactions of porphyrins with azomethine ylides. J. Org. Chem. 2005, 70, 2306–2314. [PubMed: 15760219]

(15). Zeglis BM; Brand C; Abdel-Atti D; Carnazza KE; Cook BE; Carlin S; Reiner T; Lewis JS Optimization of a Pretargeted Strategy for the PET Imaging of Colorectal Carcinoma via the Modulation of Radioligand Pharmacokinetics. Mol. Pharmaceutics 2015, 12, 3575–3587.

(16). Gonzales J; Hernandez-Gil J; Wilson TC; Adilbay D; Cornejo M; de Souza D; Franca P; Guru N; Schroeder CI; King GF; Lewis JS; et al. Bimodal Imaging of Mouse Peripheral Nerves with Chlorin Tracers. Mol. Pharmaceutics 2021, 18, 940–951.

(17). Wang T; Wang S; Liu Z; He Z; Yu P; Zhao M; Zhang H; Lu L; Wang Z; Wang Z; et al. A hybrid erbium(III)-bacteriochlorin near-infrared probe for multiplexed biomedical imaging. Nat. Mater. 2021, 20, 1571–1578. [PubMed: 34326504]

(18). Shi J; Liu TW; Chen J; Green D; Jaffray D; Wilson BC; Wang F; Zheng G Transforming a Targeted Porphyrin Theranostic Agent into a PET Imaging Probe for Cancer. Theranostics 2011, 1, 363–370. [PubMed: 21938264]

(19). Ali H; van Lier JE Metal complexes as photo- and radiosensitizers. Chem. Rev. 1999, 99, 2379–2450. [PubMed: 11749485]

(20). Bases R; Brodie SS; Rubenfeld S Attempts at tumor localization using Cu 64-labeled copper porphyrins. Cancer 1958, 11, 259–263. [PubMed: 13511344]

(21). Gomer CJ; Dougherty TJ Determination of [3H]- and [14C]hematoporphyrin derivative distribution in malignant and normal tissue. Cancer Res. 1979, 39, 146–151. [PubMed: 761185]

(22). Mercer-Smith JA; Cole DA; Roberts JC; Lewis D; Behr MJ; Lavallee DK The biodistribution of radiocopper-labeled compounds. Adv. Exp. Med. Biol. 1989, 258, 103–121. [PubMed: 2626980]

(23). Kim HJ; Lindsey JS De novo synthesis of stable tetrahydroporphyrinic macrocycles: bacteriochlorins and a tetradehydrocorrin. J. Org. Chem. 2005, 70, 5475–5486. [PubMed: 15989329]

(24). Huang YY; Balasubramanian T; Yang E; Luo D; Diers JR; Bocian DF; Lindsey JS; Holten D; Hamblin MR Stable synthetic bacteriochlorins for photodynamic therapy: role of dicyano peripheral groups, central metal substitution (2H, Zn, Pd), and Cremophor EL delivery. ChemMedChem 2012, 7, 2155–2167. [PubMed: 23065820]

(25). Gonzales J; Bhupathiraju NV; Perea W; Chu H; Berisha N; Bueno V; Dodic N; Rozenberg J; Greenbaum NL; Drain CM Facile synthesis of chlorin bioconjugates by a series of click reactions. Chem. Commun. 2017, 53, 3773–3776.

(26). Mitra S; Foster TH In vivo confocal fluorescence imaging of the intratumor distribution of the photosensitizer mono-L-aspartyl-chlorin-e6. Neoplasia 2008, 10, 429–438. [PubMed: 18472960]

(27). Hamblin MR; Rajadhyaksha M; Momma T; Soukos NS; Hasan T In vivo fluorescence imaging of the transport of charged chlorin e6 conjugates in a rat orthotopic prostate tumour. Br. J. Cancer 1999, 81, 261–268. [PubMed: 10496351]

(28). Tanaka M; Kataoka H; Mabuchi M; Sakuma S; Takahashi S; Tujii R; Akashi H; Ohi H; Yano S; Morita A; et al. Anticancer effects of novel photodynamic therapy with glycoconjugated chlorin for gastric and colon cancer. Anticancer Res. 2011, 31, 763–769. [PubMed: 21498693]

(29). Le NA; Babu V; Kalt M; Schneider L; Schumer F; Spingler B Photostable Platinated Bacteriochlorins as Potent Photodynamic Agents. J. Med. Chem. 2021, 64, 6792–6801. [PubMed: 33988998]

(30). Van Eldik R; Stochel G Inorganic Photochemistry; Academic Press, 2011, vol 63.

(31). Pandey G; Banerjee P; Gadre SR Construction of enantiopure pyrrolidine ring system via asymmetric [3+2]-cycloaddition of azomethine ylides. Chem. Rev. 2006, 106, 4484–4517. [PubMed: 17091927]

(32). (a)Zhang S; Lindsey JS Construction of the Bacteriochlorin Macrocycle with Concomitant Nazarov Cyclization To Form the Annulated Isocyclic Ring: Analogues of Bacteriochlorophyll a. J. Org. Chem. 2017, 82, 2489–2504. [PubMed: 28225270] (b)Guberman-Pfeffer MJ; Greco JA; Samankumara LP; Zeller M; Birge RR; Gascon JA; Bruckner C Bacteriochlorins with a Twist: Discovery of a Unique Mechanism to Red-Shift the Optical Spectra of Bacteriochlorins. J. Am. Chem. Soc 2007, 139, 548–560.

(33). King GF; Vetter I No gain, no pain: NaV1.7 as an analgesic target. ACS Chem. Neurosci 2014, 5, 749–751. [PubMed: 25111714]

(34). Sangameswaran L; Fish LM; Koch BD; Rabert DK; Delgado SG; Ilnicka M; Jakeman LB; Novakovic S; Wong K; Sze P; et al. A novel tetrodotoxin-sensitive, voltage-gated sodium channel expressed in rat and human dorsal root ganglia. J. Biol. Chem. 1997, 272, 14805–14809. [PubMed: 9169448]

(35). Klint JK; Smith JJ; Vetter I; Rupasinghe DB; Er SY; Senff S; Herzig V; Mobli M; Lewis RJ; Bosmans F; et al. Seven novel modulators of the analgesic target NaV 1.7 uncovered using a high-throughput venom-based discovery approach. Br. J. Pharmacol. 2015, 172, 2445–2458. [PubMed: 25754331]

(36). Gonzales J; Pirovano G; Chow CY; de Souza Franca PD; Carter LM; Klint JK; Guru N; Lewis JS; King GF; Reiner T Fluorescence labeling of a NaV1.7-targeted peptide for near-infrared nerve visualization. EJNMMI Res. 2020, 10, 49. [PubMed: 32409881]

(37). Gonzales J; Bhupathiraju N; Hart D; Yuen M; Sifuentes MP; Samarxhiu B; Maranan M; Berisha N; Batteas J; Drain CM One-Pot Synthesis of Four Chlorin Derivatives by a Divergent Ylide. J. Org. Chem. 2018, 83, 6307–6314. [PubMed: 29775305]

(38). Gonzales J; de Souza D; Franca P; Jiang Y; Pirovano G; Kossatz S; Guru N; Yarilin D; Agwa AJ; Schroeder CI; Patel SG; et al. Fluorescence Imaging of Peripheral Nerves by a Nav1.7-Targeted Inhibitor Cystine Knot Peptide. Bioconjugate Chem. 2019, 30, 2879–2888.

(39). Hoehne A; Behera D; Parsons WH; James ML; Shen B; Borgohain P; Bodapati D; Prabhakar A; Gambhir SS; Yeomans DC; et al. A 18F-labeled saxitoxin derivative for in vivo PET-MR imaging of voltage-gated sodium channel expression following nerve injury. J. Am. Chem. Soc. 2013, 135, 18012–18015. [PubMed: 24261833]

(40). Meyer RA; Bagheri SC Microsurgical reconstruction of the trigeminal nerve. Oral Maxillofac. Surg. Clin. North Am. 2013, 25, 287–302. [PubMed: 23510602]

(41). Boyd KU; Nimigan AS; Mackinnon SE Nerve reconstruction in the hand and upper extremity. Clin. Plast. Surg. 2011, 38, 643–660. [PubMed: 22032591]

(42). Li Y; Chen Q; Pan X; Lu W; Zhang J Development and Challenge of Fluorescent Probes for Bioimaging Applications: From Visualization to Diagnosis. Top Curr. Chem. 2022, 380, 22.

(43). Grootendorst MR; Cariati M; Kothari A; Tuch DS; Purushotham A Cerenkov luminescence imaging (CLI) for image-guided cancer surgery. Clin. Transl. Imaging 2016, 4, 353–366. [PubMed: 27738626]

(44). Jiménez-Osés G; García JI; Silva AMG; Santos ARN; Tomé AC; Neves MGPMS; Cavaleiro JAS Mechanistic insights on the site selectivity in successive 1,3-dipolar cycloadditions to meso-tetraarylporphyrins. Tetrahedron 2008, 64, 7937–7943.

(45). Silva AMG; Tomé AC; Neves MGPMS; Silva AMS; Cavaleiro JAS meso-Tetraarylporphyrins as dipolarophiles in 1,3-dipolar cycloaddition reactions. Chem. Commun. 1999, 1767–1768.

(46). Singh S; Aggarwal A; Bhupathiraju NV; Arianna G; Tiwari K; Drain CM Glycosylated Porphyrins, Phthalocyanines, and Other Porphyrinoids for Diagnostics and Therapeutics. Chem. Rev. 2015, 115, 10261–10306. [PubMed: 26317756]

(47). Echternach M; Maurer CA; Mencke T; Schilling M; Verse T; Richter B Laryngeal complications after thyroidectomy: is it always the surgeon? Arch. Surg. 2009, 144, 149–153. [PubMed: 19221326]

(48). Gordin E; Lee TS; Ducic Y; Arnaoutakis D Facial nerve trauma: evaluation and considerations in management. Craniomaxillofac. Trauma Reconstr. 2015, 8, 1–13. [PubMed: 25709748]

(49). Elkahwagi M; Salem MA; Moneir W; Allam H Traumatic facial nerve paralysis dilemma. Decision making and the novel role of endoscope. J. Otol. 2022, 17, 116–122. [PubMed: 35847576]

(50). Klint JK; Senff S; Saez NJ; Seshadri R; Lau HY; Bende NS; Undheim EA; Rash LD; Mobli M; King GF Production of recombinant disulfide-rich venom peptides for structural and functional analysis via expression in the periplasm of E. coli. PLoS One 2013, 8, No. e63865.

(51). Jiang Y; Castro J; Blomster LV; Agwa AJ; Maddern J; Schober G; Herzig V; Chow CY; Cardoso FC; De Souza D; Franca P; et al. Pharmacological Inhibition of the Voltage-Gated Sodium Channel NaV1.7 Alleviates Chronic Visceral Pain in a Rodent Model of Irritable Bowel Syndrome. ACS Pharmacol. Transl. Sci. 2021, 4, 1362–1378. [PubMed: 34423271]

(52). Reiner T; Thurber G; Gaglia J; Vinegoni C; Liew CW; Upadhyay R; Kohler RH; Li L; Kulkarni RN; Benoist C; et al. Accurate measurement of pancreatic islet beta-cell mass using a second-generation fluorescent exendin-4 analog. Proc. Natl. Acad. Sci. U. S. A. 2011, 108, 12815–12820. [PubMed: 21768367]

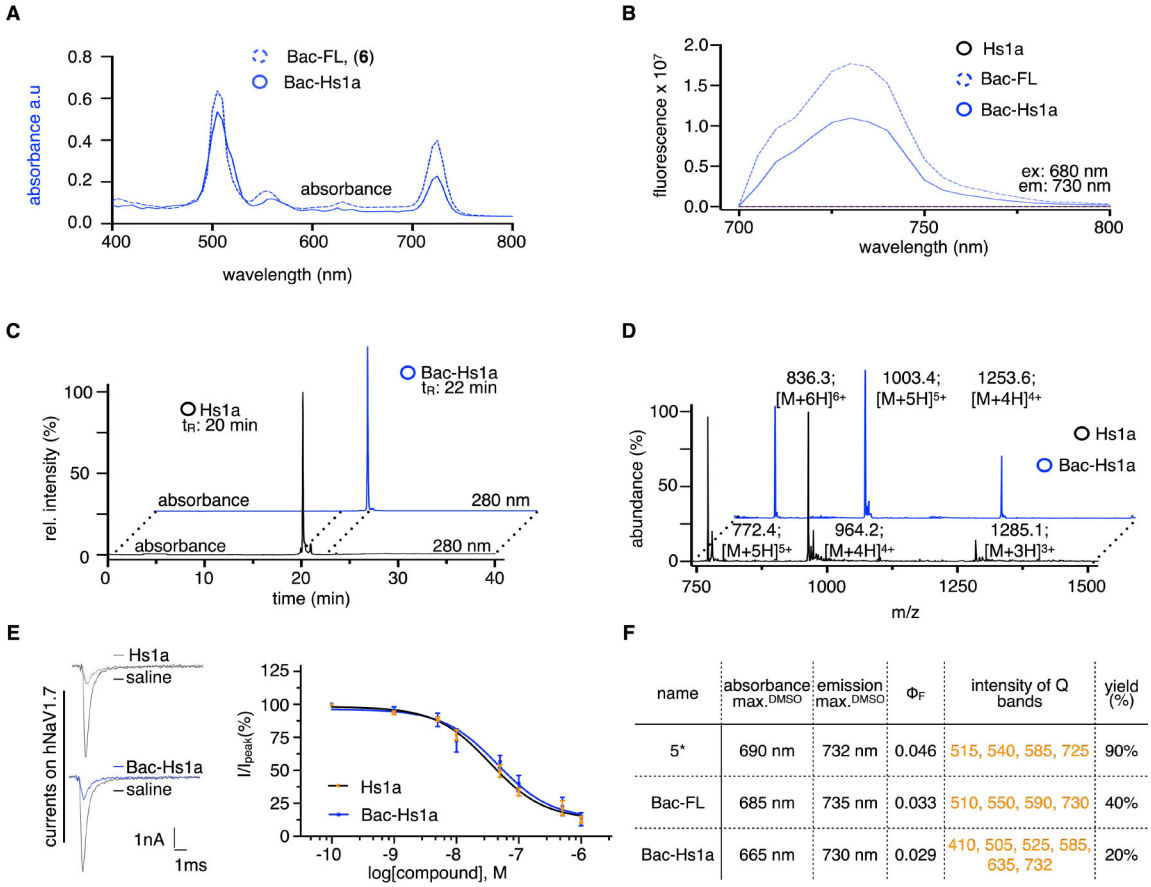

name	absorbance max.DMSO	emission max.DMSO	Φ_F	intensity of Q bands	yield (%)
5*	690 nm	732 nm	0.046	515, 540, 585, 725	90%
Bac-FL	685 nm	735 nm	0.033	510, 550, 590, 730	40%
Bac-Hs1a	665 nm	730 nm	0.029	410, 505, 525, 585, 635, 732	20%

Figure 1.

Photochemical features, affinity, and validation of bacteriochlorin-based tracers. (A) Absorbance spectra of 0.1 μM compound 6 (dashed blue) and Bac-Hs1a (solid blue), observed from 400–800 nm, and where the classical 730 nm bacteriochlorin peak was detected. (B) Fluorescence spectra of 0.1 μM Hs1a (black), 0.1 μM Bac-FL (dashed blue), and 0.1 μM Bac-Hs1a (solid blue), observed at a range of 700–800 nm, and the classical bacteriochlorin emission wavelength at 730 nm, where the excitation was 680 nm. (C) RP-HPLC chromatograms of the Hs1a peptide (black) and the fluorescent Bac-Hs1a tracer (blue), with retention times of 20 and 22 min, respectively, observed at 280 nm absorption. (D) LC–MS spectra of Bac-Hs1a and Hs1a peptides, showing major ion species that correspond to the calculated mass of the synthetic Hs1a and the fluorescent Bac-Hs1a. (E) Effect of Hs1a and Bac-Hs1a peptides on human NaV1.7. Representative currents of human NaV1.7 (left) in the presence of 500 nM Hs1a (top) or 500 nM Bac-Hs1a (bottom). In addition, a fit of the Hill equation to concentration–response curves (right) showing inhibition by Hs1a (IC_{50} = 34.9 ± 7.0 nM; n = 7) and Bac-Hs1a (IC_{50} = 45.2 ± 14.0 nM; n = 6). The peak current amplitude recorded after peptide treatment was normalized to the maximum peak current from the same cell in the absence of the peptide. (F) Exclusive features of compound **5**, Bac-FL (6), and Bac-Hs1a comprising absorbance and emission maxima, quantum yields, individual yields, intensity of Q bands, and obtained yields.

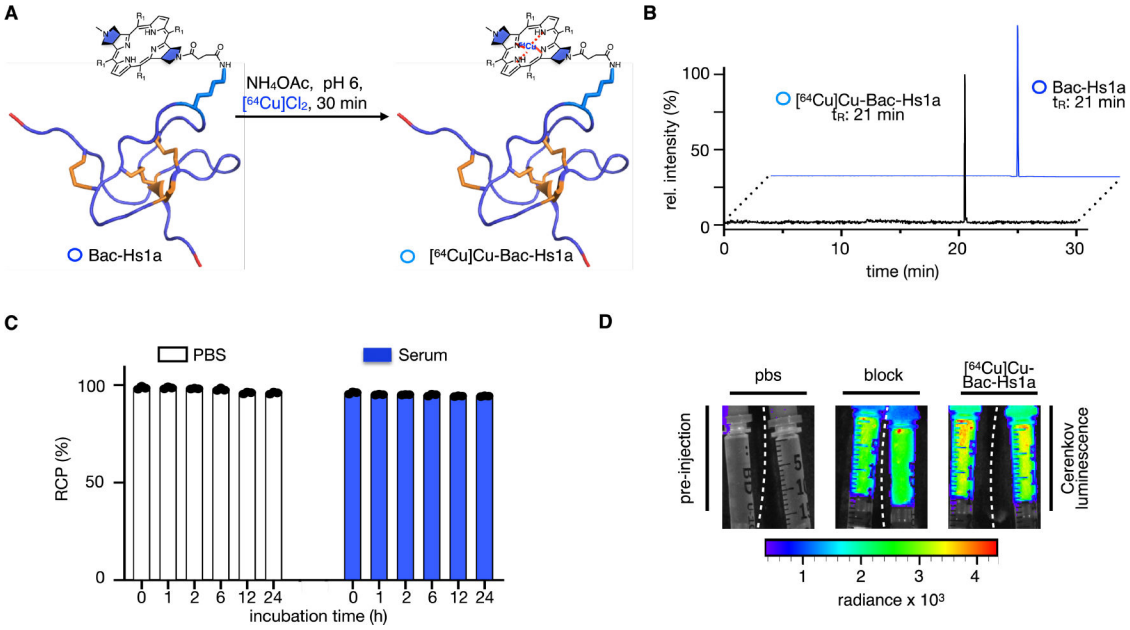

Figure 2.

Radiolabeling, characterization, and stability of bacteriochlorin-based tracers. (A) Radiochemical synthesis via the chelation of the bacteriochlorin with ^{64}Cu to afford the [^{64}Cu]Cu-Bac-Hs1a radiotracer, a radiolabeling that takes place in slightly acidic pH in around 30 min. (B) Radio-HPLC chromatogram of a labeled [^{64}Cu]Cu-Bac-Hs1a at 37 °C for 30 min with a corresponding HPLC chromatogram of the cold Bac-Hs1a standard at 280 nm absorption. (C) Radio-HPLC experiments for stability of [^{64}Cu]Cu-Bac-Hs1a in saline and serum solution(s), (RCP = the radiochemical purity of [^{64}Cu]Cu-Bac-Hs1a, $n = 3$). (D) Cerenkov luminescence of the formulated [^{64}Cu]Cu-Bac-Hs1a and block formulation after radiochemical synthesis before injection.

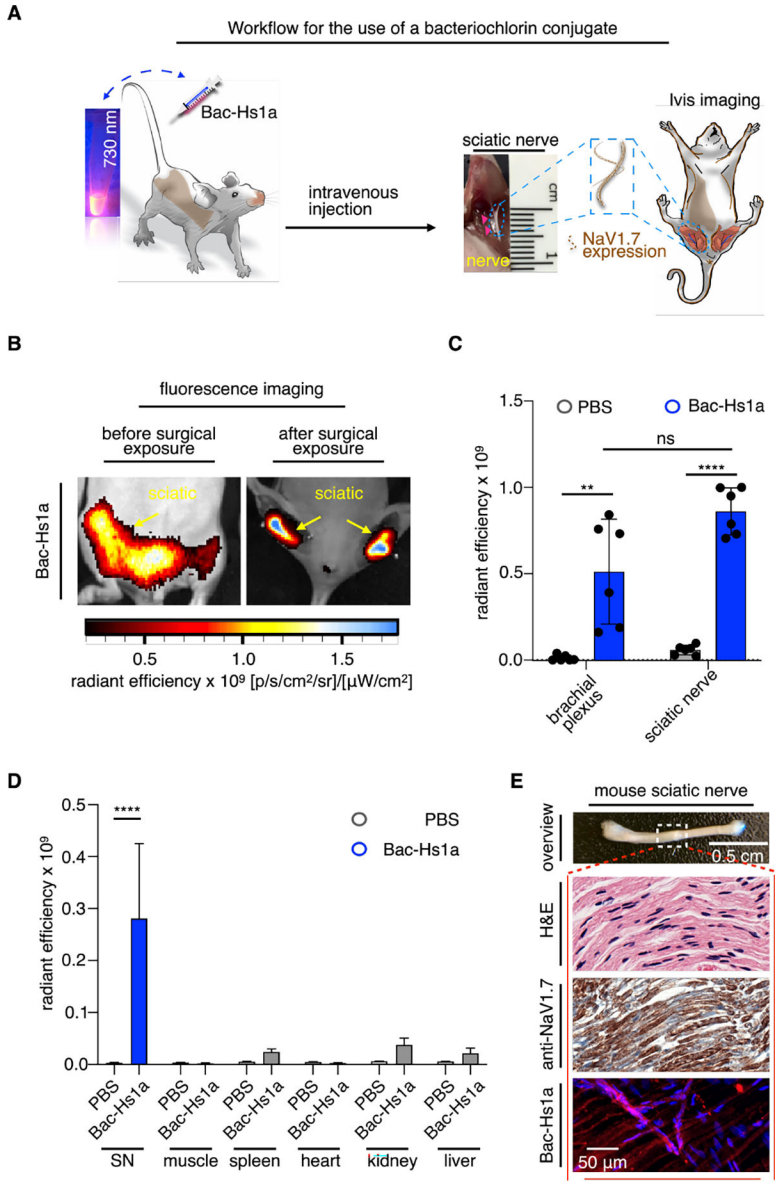

Figure 3.

Surgical exposure and Bac-Hs1a accumulation in mouse peripheral nerves and corresponding microscopy. (A) Workflow for the fluorescence in vivo experiments of the engineered contrast agent based on a bacteriochlorin molecule. Bac-Hs1a targets sodium channel NaV1.7 highly expressed on peripheral nerves. (B) Epifluorescence images (pre- and post-nerve-exposure) of animals injected with fluorescent agent Bac-Hs1a (1 nmol, 11 μM of Bac-Hs1a in 100 μL PBS) show highlighted nerve tissue on the upper and lower body. Images were taken after 30 min of tail vein injection. (C) Fluorescence intensity semi-quantification of Figure 3B. Statistics were calculated with parametric Student's *t* test. $^{**}P < 0.01$; $^{****}P < 0.0001$; and NS, not significant. (D) Biodistribution quantification of mouse peripheral nerves and corresponding organs that were injected with PBS and Bac-Hs1a. High fluorescence intensities, due to bacteriochlorin-Hs1a conjugate accumulation, were only observed in peripheral nerves injected with Bac-Hs1a. No fluorescence was observed

after 30 min in mice injected with the vehicle, except for Bac-Hs1a injected spleen, kidney, and liver. (E) Bac-Hs1a uptake was validated in mouse sciatic nerve (first row) fresh tissue from mice injected with Bac-Hs1a (1 nmol, 11 μM of Bac-Hs1a in 100 μL of PBS), where the control was animals injected with 100 μL of PBS. Hoechst 33342 (blue, 20 μM, 1 nmol in 50 μL of PBS) was used to light up Schwann cell nuclei. Adjacent slides were stained with H&E (second row) and anti-NaV1.7 (third row) to validate the topology of the mouse peripheral sciatic nerve. Fluorescence elongated neurons lighted up (fourth row).

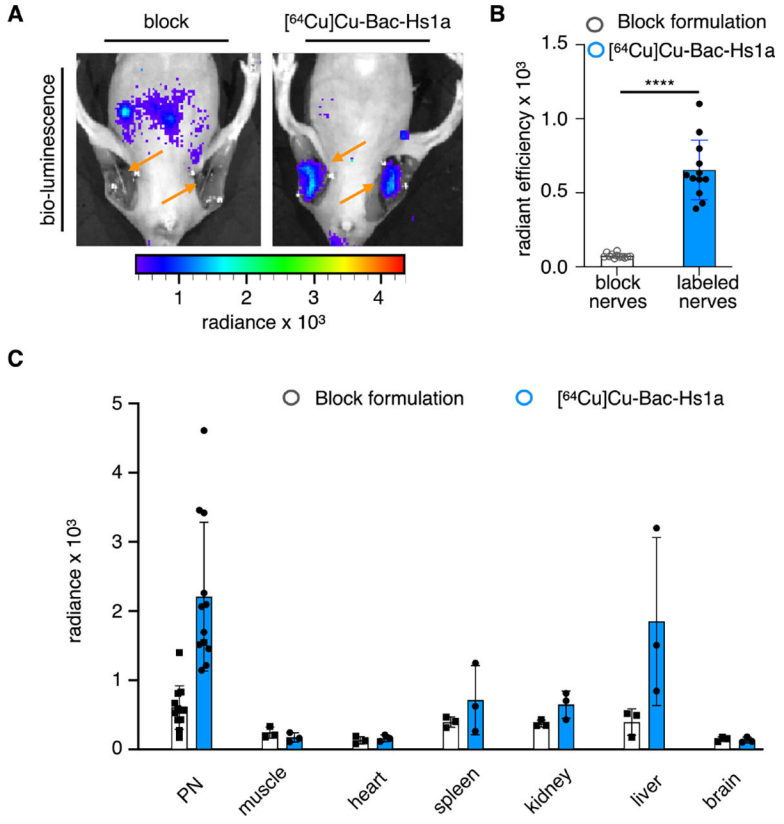

Figure 4.

Cerenkov luminescence of [^{64}Cu]Cu-Bac-Hs1a, quantification, and biodistribution. (A) Cerenkov luminescence images of mice injected with a block formulation (Hs1a and [^{64}Cu]Cu-Bac-Hs1a (left) or [^{64}Cu]Cu-Bac-Hs1a alone (right)). High radiance was observed in peripheral nerves (PN) after 30 min in mice injected with [^{64}Cu]Cu-Bac-Hs1a alone. (B) Cerenkov luminescence quantification of Figure 4A. (C) Cerenkov luminescence radiance quantification of peripheral nerves, muscle, spleen, heart, kidney, liver, and brain of mice injected with a block formulation and [^{64}Cu]Cu-Bac-Hs1a. Statistics were calculated with parametric Student's *t* test. **** $P < 0.0001$.

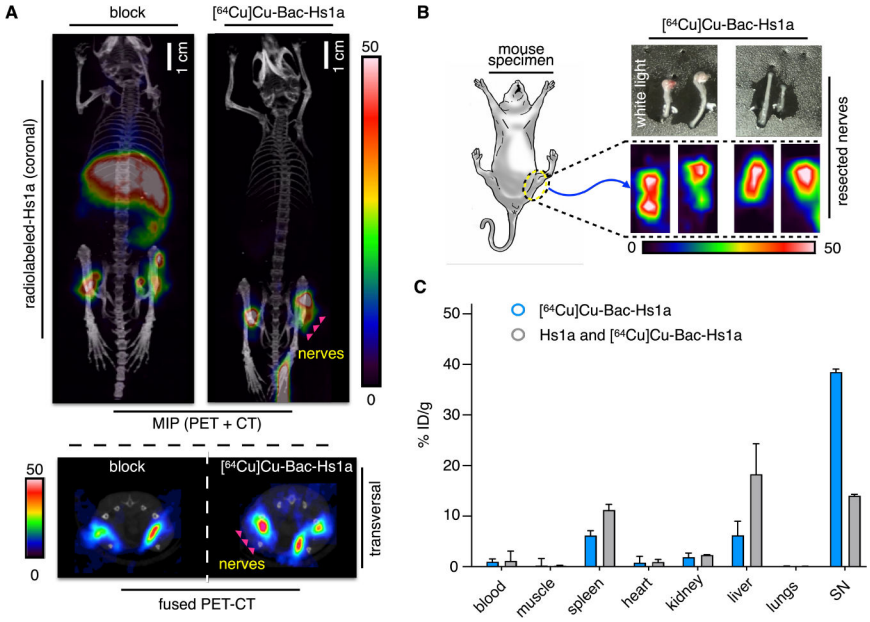

Figure 5.

PET imaging of [^{64}Cu]Cu-Bac-Hs1a in mice, PET signal of resected nerves, and biodistribution quantification. (A) Representative coronal (top) and single transversal (bottom, fused) PET/CT images of mice injected with [^{64}Cu]Cu-Bac-Hs1a (3.2–4.2 MBq in 150 μL of PBS) or a block formulation (Hs1a and [^{64}Cu]Cu-Bac-Hs1a in 150 μL of PBS). A high %ID/g is observed after 60 min in mice injected with a radiotracer alone. In addition, for the block formulation, some %ID/g is observed in nerves, spleen, and liver after 60 min as well. (B) PET images of resected nerves from animals injected with radiotracer [^{64}Cu]Cu-Bac-Hs1a. (C) PET imaging quantification (%ID/g) of sciatic nerves, muscle, spleen, heart, kidney, liver, and brain of mice injected with the block formulation and [^{64}Cu]Cu-Bac-Hs1a. Statistics were calculated with parametric Student's *t* test. *$P <$ 0.05; **$P < 0.01$; ***$P < 0.001$; ****$P < 0.0001$.

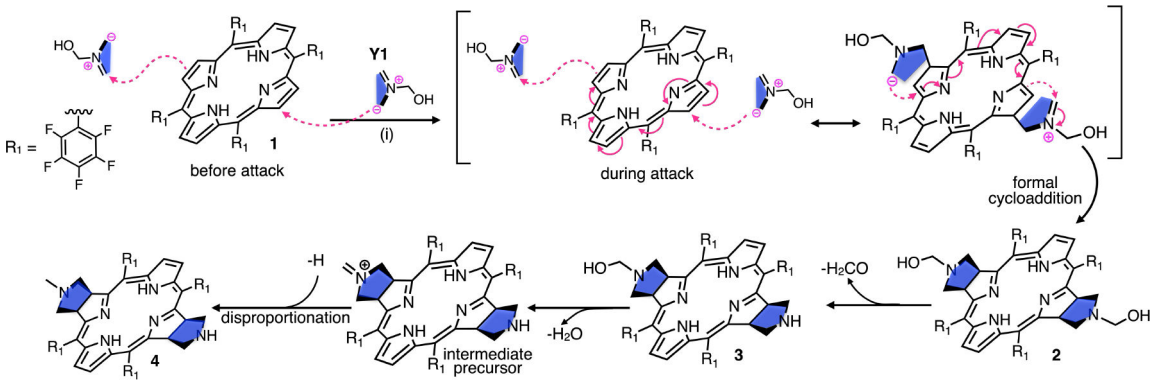

Scheme 1. Mechanism To Form Conjugable Bacteriochlorin Sensors via Formal Cycloaddition[a]

[a]This synthetic scheme mechanism for bacteriochlorin formation includes a transformation that generates solvent effects and resonance for inducement of formal cycloaddition. This trimolecular reaction begins with the **Y1** attack and resonance on the porphyrin core to generate an aromatic substitution attack to a second **Y1**, which forms and initiates the first pyrrolidine and resonance, finally closing the second pyrrolidine ring and generating the bacteriochlorin. The compound formed is 2, which loses an aldehyde and water. The final step is a disproportionation reaction that affords compound 4. In this reaction, (i) mixed-grinded ylide comprised of glycine/paraformaldehyde (1:2), with aliquots added constantly over at least 10 h in DMF, 150–170 °C, 24–36 h, 20% yield.

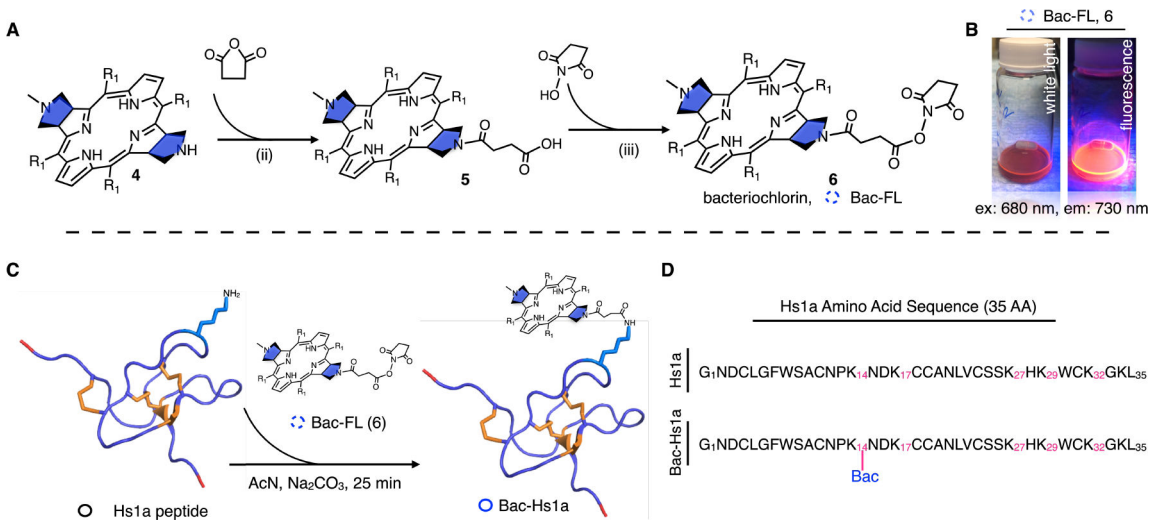

Scheme 2. Synthesis and Characterization of Bac-FL, Bac-Hs1a, and Amino Acid Sequence[a]

[a](A) Synthetic scheme of a bacteriochlorin sensor and the activation with an NHS-ester moiety that provides target specificity when conjugated to a targeting molecule. To compound 4, (ii) 6 equiv succinic anhydride, DCM, NEt_3, room temperature, 45 min, 90% yield. (iii) 1.2 equiv *N*-hydroxysuccinimide, THF, 1.1 equiv DCC, r.t., 30% yield. (B) Bacteriochlorin-based molecules under white light (left) and under excitation at 680 nm (right), formulated in PBS for intravenous injection. (C) Reaction scheme for the covalent conjugation of the bacteriochlorin moiety to the Hs1a peptide under basic conditions to afford Bac-Hs1a. The ribbon model of Bac-Hs1a shows disulfide bridges (in orange), the amino acid sequence (purple), and the bacteriochlorin (black), a conjugation that takes place in at least 10 min. (D) Amino acid sequences of Hs1a and Bac-Hs1a peptides containing 35 amino acids; Bac-Hs1a contains a bacteriochlorin molecule at K_{14}. The connectivity (in orange) for the cystines in Hs1a is C_4–C_{19}, C_{11}–C_{24}, and C_{18}–C_{31}.